Bio-Design and Manufacturing (2020) 3:383–395
https://doi.org/10.1007/s42242-020-00092-6

RESEARCH ARTICLE

Cigarette smoke-induced malignant transformation via STAT3 signalling in pulmonary epithelial cells in a lung-on-a-chip model

Wei Hou[1,2] · Siyi Hu[1] · Ken-tye Yong[3] · Jie Zhang[2] · Hanbin Ma[1]

Received: 21 February 2020 / Accepted: 3 August 2020 / Published online: 17 August 2020

Abstract

Background Chronic obstructive pulmonary disease (COPD) is a severe public health problem. Cigarette smoke (CS) is a risk factor for COPD and lung cancer. The underlying molecular mechanisms of CS-induced malignant transformation of bronchial epithelial cells remain unclear. In this study, we describe a lung-on-a-chip to explore the possible mechanistic link between cigarette smoke extract (CSE)-associated COPD and lung cancer.

Methods An in vitro lung-on-a-chip model was used to simulate pulmonary epithelial cells and vascular endothelial cells with CSE. The levels of IL-6 and TNF-α were tested as indicators of inflammation using an enzyme-linked immune sorbent assay. Apical junction complex mRNA expression was detected with qRT-PCR as the index of epithelial-to-mesenchymal transition (EMT). The effects of CSE on the phosphorylation of signal transduction and transcriptional activator 3 (STAT3) were detected by Western blotting. Flow cytometry was performed to investigate the effects of this proto-oncogene on cell cycle distribution.

Results Inflammation caused by CSE was achieved in a lung-on-a-chip model with a mimetic movement. CSE exposure induced the degradation of intercellular connections and triggered the EMT process. CSE exposure also activated the phosphorylation of proto-oncogene STAT3, while these effects were inhibited with HJC0152.

Conclusions CSE exposure in the lung-on-a-chip model caused activation of STAT3 in epithelial cells and endothelial cells. HJC0152, an inhibitor of activated STAT3, could be a potential treatment for CS-associated COPD and lung cancer.

Keyword Cigarette smoke · Microfluidic chips · STAT3 · Chronic obstructive pulmonary disease

Abbreviations

NSCLC	Non-small cell lung cancer
COPD	Chronic obstructive pulmonary disease
EGFR	Epidermal growth factor receptor
STAT3	Signal transduction and transcriptional activators 3
PDMS	Polydimethylsiloxane
ICAM	Intercellular cell adhesion molecule
CAFs	Cancer-associated fibroblasts
IL-6	Interleukin-6
IFP	Interstitial fluid pressure
ZOs	Zonula occludens
EMT	Epithelial–mesenchymal transformation
AJC	Apical junctional complex
VCAM	Vascular cell adhesion molecule
α-SMA	Alpha smooth muscle actin
VEGF	Vascular endothelial growth factor
ALK	Anaplasticlymphoma kinase
SOCS	Suppressor of cytokine signalling
EndMT	Endothelial–mesenchymal transition

Wei Hou and Siyi Hu contribute equally to this article.

✉ Jie Zhang
zjie99@jlu.edu.cn

✉ Hanbin Ma
mahb@sibet.ac.cn

[1] CAS Key Laboratory of Bio-Medical Diagnostics, Suzhou Institute of Biomedical Engineering and Technology, Chinese Academy of Sciences, No.88 Keling Road, Huqiu District, Suzhou 215163, Jiangsu, People's Republic of China

[2] Department of Respiratory and Critical Care Medicine, The Second Hospital of Jilin University, No.218 Ziqiang Street, Nanguan District, Changchun 130041, Jilin, People's Republic of China

[3] School of Electrical and Electronic Engineering, Nanyang Technological University, Singapore 639798, Singapore

Background

Chronic obstructive pulmonary disease (COPD), a group of diseases causing airflow blockage, is commonly associated with prolonged exposure to toxic aerosols [1]. Cigarette smoke (CS), a mixture of approximately 4,500 components (e.g. carbon oxide nicotine, oxidants, fine particulate matter and aldehydes), is the major factor that contributes to the pathogenesis and progression of COPD [2, 3]. Smoking and aberrant epithelial responses are risk factors for COPD and lung cancer [4]. In the past decades, enormous effort has been made in the research and development of drugs such as novel immunotherapies and molecularly targeted agents, which improves the prognosis in lung cancer patients to some extent. However, it remains one of the major causes of cancer-related death worldwide [5, 6]. To date, extensive studies have been conducted to investigate the molecular mechanisms that prolong CS-induced malignant transformation of bronchial epithelial cells. Several aspects are considered to be crucial in this process, including DNA damage, epithelial-to-mesenchymal transition (EMT), as well as aberrant cell proliferation and tissue repair [7–10]. Many animal models and in vitro models have been established in this field, but their limitations may restrict the significance of their findings [5, 11, 12]. For example, the respiratory system of rodents is widely divergent from that of humans, and the monolayer static cell culture cannot mimic the complex microenvironment of pulmonary structure [13, 14]. Airway epithelial barrier dysfunction is associated with the pathogenesis of inflammation [15], and micro-vascular endothelium acts as an important mediator in this process [16]. In addition, tumour tissue is closely related to hyper-angiogenesis [17]. These findings suggest that vascular endothelium is responsible for the pathological process of COPD and lung cancer.

Microfluidic 3D culture system is a practical tool for in vitro modelling of complex human physiology mimicking the carcinogenesis of epithelial tissue in a structurally appropriate context [18]. The organ surrogate device is also known as organ-on-chip [19, 20] that has been widely used in biomedical research as it can effectively predict human responses and simultaneously reduce animal experiments with moral controversy. As a organ-on-chip, lung-on-a-chip has been reported to reconstruct the active terminal bronchus-vascular interface of human lung and focus on the inflammatory reaction caused by cytokines and toxic nanoparticles [21]. In this article, we fabricated a lung-on-a-chip model of breathing lung containing vascular endothelium and bronchial epithelium, in order to mimic the microenvironment of the air–blood interface with a porous membrane for breathing lung. We aim to investigate the possible role of STAT3 phosphorylation in cigarette smoke associated COPD and the malignant transformation of bronchial epithelium.

Methods

Design and fabrication of microfluidic chip

The 2D hexagonal microfluidic chip was designed based on four modules shown in Fig. 1. The lung-on-a-chip device was fabricated through conventional soft-lithography and replica-moulding methods as previously described [22]. Four modules were made with polydimethylsiloxane (PDMS, Dow Corning, Michigan, USA). Briefly, negative photoresistant SU-8 was spin coated onto a silicon wafer, followed by UV patterning of the chamber structure and micro-porous array to form a model. The PDMS mixture containing curing agent and base resin (weight ratio, 1:10) was poured onto the SU-8 models cured at 90 °C for 30 min. The cured PDMS layer with microstructures was then carefully peeled off from the model and fabricated together. The pneumatic chamber showed a hexagonal border with a column on the side that created mechanical deformation with periodic suction of air. The liquid channel and air channel were micro-pillar array substrates, with a membrane (thickness, 40 μm; porous diameter of 10 μm) localizing between them (Fig. 1). Air chamber and liquid chamber contained a micro-pillar array with the same volume (diameter, 100 μm; height, 200 μm, the distance between adjacent pillar centres, 400 μm). On this basis, the space between adjacent micro-pillars was approximately equal to the average volume of a terminal bronchus [21, 23].

Cell culture

Two different cell lines were used in this study. Human bronchial epithelium BEAS-2B cells were purchased from the American Type Culture Collection (ATCC; Manassas, VA, USA). Human vascular endothelial cells (HUVECs) were provided by China Cell Line Bank (Beijing, China). Cells were resuscitated and cultured in DMEM complete medium containing 10% foetal bovine serum (FBS, Gibco, USA). The porous membranes were coated with type I collagen (Yeasen, Shanghai, China), followed by adding the epithelial cells and endothelial cells into the air chamber and liquid chamber. The BEAS-2B cell suspension was added into the air chamber, which promoted the cellular adhesion to the membrane. Subsequently, the device was turned over, and then the HUVECs were added to the liquid chamber. The cell culture was removed from the air chamber and the chip was connected with a digital control pump (RSP04-B, Ristron, Jiaxing, China). Medium was

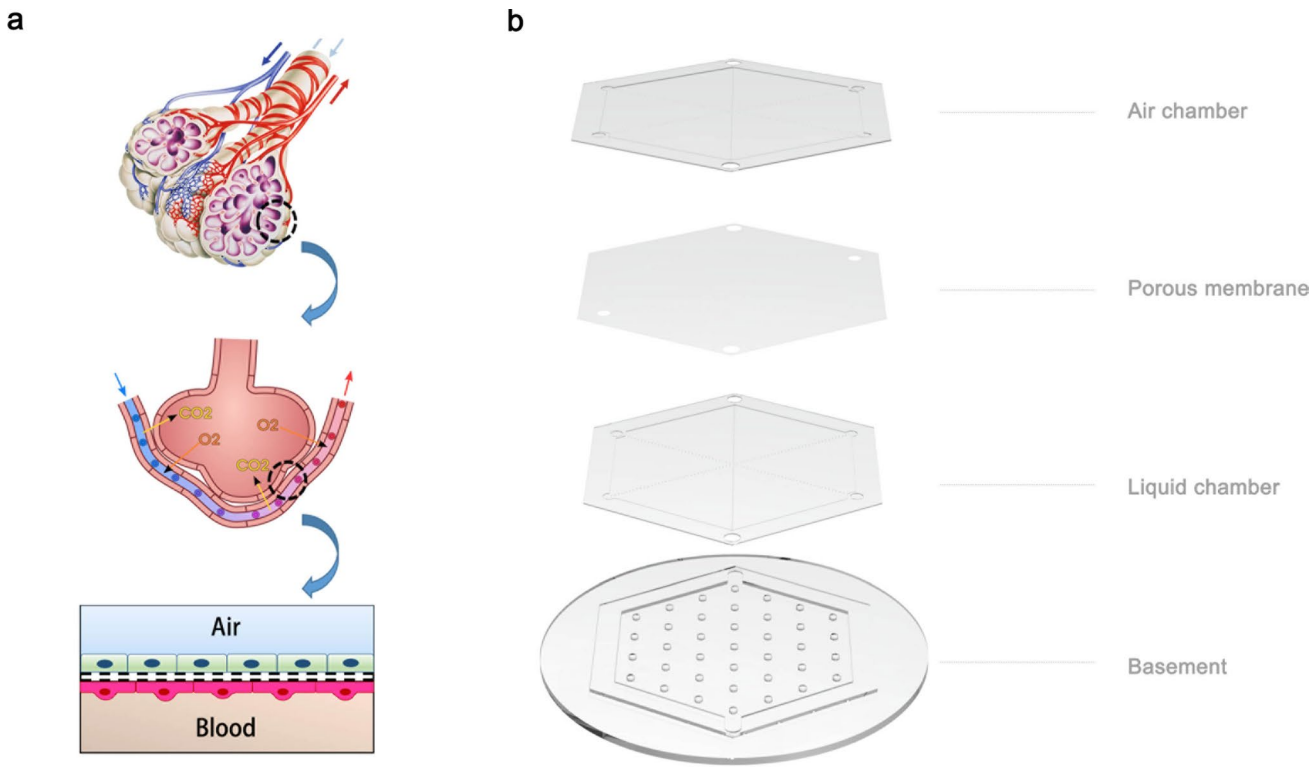

Fig. 1 **a** The structure of human terminal bronchus, air–liquid interface and simplified diagrammatic view of the microenvironment. **b** Blueprint of lung-on-a-chip

pumped into the liquid chamber in a continuous manner. BEAS-2B cell viability was maintained in the air–liquid interface until the cells attached to the opposite surfaces of the membrane, forming 75% continuous monolayers.

CSE exposure on a chip

BEAS-2B cell suspension was introduced into the air chamber using a digital syringe pump in a perfusion mode. After 12 h, the chip and HUVEC suspension were introduced into the liquid chamber. Cells were supplied with complete medium in liquid chamber at a constant rate (5 μL/min). Upon a confluence of 80%, the cells were stimulated by infusion of medium and CSE into the chip. CSE exposure lasted for 8 days, during which the chip was converted together with washing the necrotic cells with a constant pump in medium (10 μL/min) for 1 h per day. After exposure, a 7-day recovery period was set with complete medium in the absence of CSE. Finally, the BEAS-2B cells and HUVECs were obtained by washing with 0.25% trypsin–EDTA for future use.

Real-time PCR

Total RNA was extracted from BEAS-2B cells using the Tri-reagent (Sigma-Aldrich, St. Louis, USA) according to the manufacturer's instructions. The cDNA was synthesized using a commercial kit (Gene Copoeia, Maryland, USA). Real-time PCR was performed in triplicate with Takara SYBR Green using a commercial kit (Takara, Kyoto, Japan). The primer sequences are displayed in Table 1. β-actin served as the internal standard.

Enzyme-linked immunosorbent assay (ELISA)

About 24 h after CSE exposure, the supernatant was collected to measure the IL-6 and tumour necrosis factor-α (TNF-α) using ELISA (mlbio, Shanghai, China). Briefly, culture medium supernatant was centrifuged at 3000 rpm for 6 min. Aliquots (50 μL) of diluted samples were then measured according to the manufacturer's instructions. The absorbance was measured at 450 nm with a microplate reader (BioTek, Winooski, VT, USA).

Table 1 Primer sequence

Gene	Sequence	Length (bp)
IL-6	(F): 5′-ATTCCTTCTTCTGGTCAGAAACC-3′	247
	(R): 5′-ACAAAGGATATTCAAACTGCATAGC-3′	
TNF-α	(F): 5′-CAGCCTCTTCTCCTTCCTGA-3′	503
	(R): 5′-GGAAGACCCCTCCCAGATAGA-3′	
CLDN-1	(F): 5′-GCTTCTCTCTGCCTTCTGGG-3′	123
	(R): 5′-TCACACGTAGTCTTTCCCGC-3′	
CLDN-7	(F): 5′-CATCGTGGCAGGTCTTGCC-3′	118
	(R): 5′-GATGGCAGGGCCAAACTCATAC-3′	
CLDN-8	(F): 5′-ACTGGTGCTGATTGTTGGAGGAG-3′	96
	(R): 5′-GTGCGATGGGAAGGTATCGAGT-3′	
OCLD	(F): 5′-CCTATAAATCCACGCCGGTTC-3′	103
	(R): 5′-TCAAAGTTACCACCGCTGCTG-3′	
CDH-5	(F): 5′-ACCGGATGACCAAGTACAGC-3′	596
	(R): 5′-ACACACTTTGGGCTGGTAGG -3′	
CDH-1	(F): 5′-CCGCCGGCGTCTGTAGGAA-3′	150
	(R): 5′-AGGGCTCTTTGACCACCGCTCTC-3′	
β-actin	(F): 5′-ACAGGAAGTCCCTTGCCATC-3′	248
	(R): 5′-AGGGAGACCAAAAGCCTTCA-3′	

Western blot analysis

Protein was extracted from the cells using RIPA lysis buffer (Beyotime, Shanghai, China). Protein concentration was determined using Pierce™ BCA Protein Assay Kit (Thermo Scientific, MA, USA). Samples (40 μg) were subjected to electrophoresis and subsequently transferred to polyvinylidene fluoride (PVDF) membranes (Millipore, Darmstadt, Germany). PVDF membranes were incubated with primary antibodies (1:1000) overnight at 4 °C, followed by horseradish peroxidase (HRP)-conjugated secondary antibodies (1:2000, Bosterbio, USA) at room temperature for 1 h. Protein bands were visualized using a Beyo Enhanced Chemiluminescence reagent kit (Beyotime, Shanghai, China). The β-actin served as the internal standard.

Cell cycle analysis

Cells were trypsinized for 3 min and washed out of the channel, resuspended and centrifuged twice with PBS. Then they were fixed in 70% ethanol overnight at 4 °C and stained with propidium iodide (PI; 5 μg/mL PI in PBS containing 0.1% Triton X-100 and 0.2 mg/mL RNase A). The cell cycle was analyzed by flow cytometry (LSRFortessa, BD, USA).

Statistics

The data were displayed as mean ± standard deviation. Data were analysed with SPSS 19.0 software (SPSS Inc., USA). The dissimilarity among groups was analysed by one-way analysis of variance (ANOVA). All bar charts were generated by GraphPad Prism (v7; GraphPad Software, USA). $P < 0.05$ was regarded to be statistically significant.

Results and discussion

Lung-on-a-chip design and cell culture

Microfluidic 3D culture systems are practical for in vitro modelling of complex human physiology mimicking the carcinogenesis of epithelial tissue in a structurally appropriate context. Such organ surrogate device is also known as organ-on-chip [19, 20]. In organ-on-chip models, remodelling normal tissue-tissue interfaces and mimicking this complex physical microenvironment in which cells were normally situated were necessary [13]. The most commonly used lung-on-a-chip model usually has a cell culture chamber (1 cm in length, 400 μm in width, and 100 μm in height) in order to mimic the terminal bronchus volume [13, 19]. The cells on our chip were adequate for immunofluorescence and ELISA. However, off-chip cell proliferation was required for experiments such as western blot and real-time PCR [24]. We fabricated a lung-on-a-chip model of breathing lung containing vascular endothelium and bronchial epithelium to mimic the microenvironment of the air–blood interface with a porous membrane for breathing lung. On this basis, we further investigated the possible mechanism that linked

CSE-associated COPD and lung cancer. The chip contained a micro-pillar array with the same volume (100 μm in diameter, 200 μm in height). The space between adjacent micro-pillars (400 μm) was approximately the average volume of terminal bronchus [21, 23]. We also expanded the area used for cell culture, which provided sufficient cells for Western blot and/or Real-Time PCR. The two chambers were separated by a porous flexible membrane made of collagen-coated PDMS. The human bronchial epithelial cell line BEAS-2B and HUVECs were introduced into the air and liquid chambers, followed by grown on the collagen-coated membrane to form two confluent monolayers, respectively. This model mimicked the physiological breathing motions of the lung, and vacuum was applied to the bottom of chambers to induce downward bending of the upper chambers, in order to mimic the stretch of the bronchus wall caused by physiological breathing motions. This distortion warped the intervening PDMS membrane along with the attached cell monolayers. Dynamic mechanical deformation was generated in the presence of vacuuming and releasing the pneumatic chamber at a frequency of 0.25 Hz, which was analogous to the deformation occurring in the pulmonary tissue of breathing human lung [14].

Figure 2 indicates the final appearance of the chip after integration. To test the device compatibility, we seeded BEAS-2B cells and HUVECs onto the chip. As shown in Fig. 3, the growth of BEAS-2B human bronchial epithelial cells and HUVECs in the device was satisfactory. The morphology of cells on the chip was similar to that of the cells in the culture flask. After cell culture in the lung-on-a-chip model for 24 h, the cell trackers were introduced for the live cell labelling. Subsequently, the BEAS-2B cells were labelled in a green color with CMFDA, and HUVECs were labelled in a red colour with cell tracker CM-Dil.

CSE triggered inflammation in lung-on-a-chip model

In our previous study [25], CSE (100 μg/mL) caused no acute cytotoxicity against BEAS-2B cells. On this basis, CSE (10 μg/mL, 20 μg/mL and 50 μg/mL) was selected for on-chip experiments to investigate whether prolonged CSE exposure in the lung-on-a-chip co-culture system of BEAS-2B cells and HUVECs could lead to malignant transformation of BEAS-2B cells.

The bronchial epithelial cell line BEAS-2B and HUVECs were cultured in flasks separately. A co-culture model of two cell lines was established using the Transwell chamber. After CSE exposure, the levels of IL-6 and TNF-α in the supernatant were measured. IL-6 and TNF-α levels in the co-culture group and the on-chip group were significantly higher than those in the single cell groups (Fig. 4a and b). The level of IL-6 in the on-chip group was higher than that of the co-culture group. There was no significant difference in the level of TNF-α between the two groups ($P > 0.05$). Our data were similar to the previous description by Benam et al. [13], indicating that the intrinsic cross-talk between human epithelium and endothelium during CSE-induced inflammation may be related to mechanical stretch. Additionally, it indicated that IL-6 and its downstream signalling pathway might play an important role in the pathological process of lung cancer induced by CSE in lung.

CSE induced lung air–blood barrier dysfunction

Lung air–blood barrier acted as the place for O_2/CO_2 exchange and the safeguard to bear the brunt of inhaled irritants. It essentially consisted of bronchus alveolar epithelium and capillary endothelium, which were connected or separated by interstitial tissue of varying composition and width

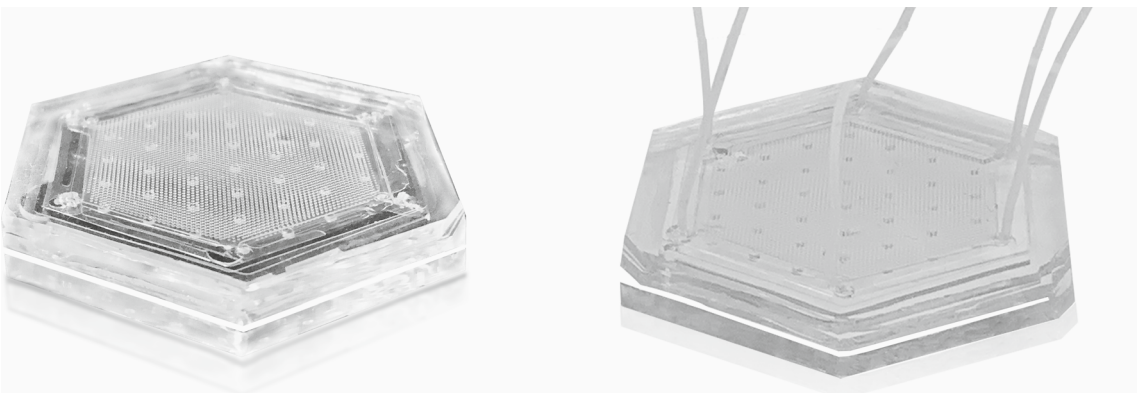

Fig. 2 The lung-on-a-chip before (left) and after (right) connection with PTFE pipe

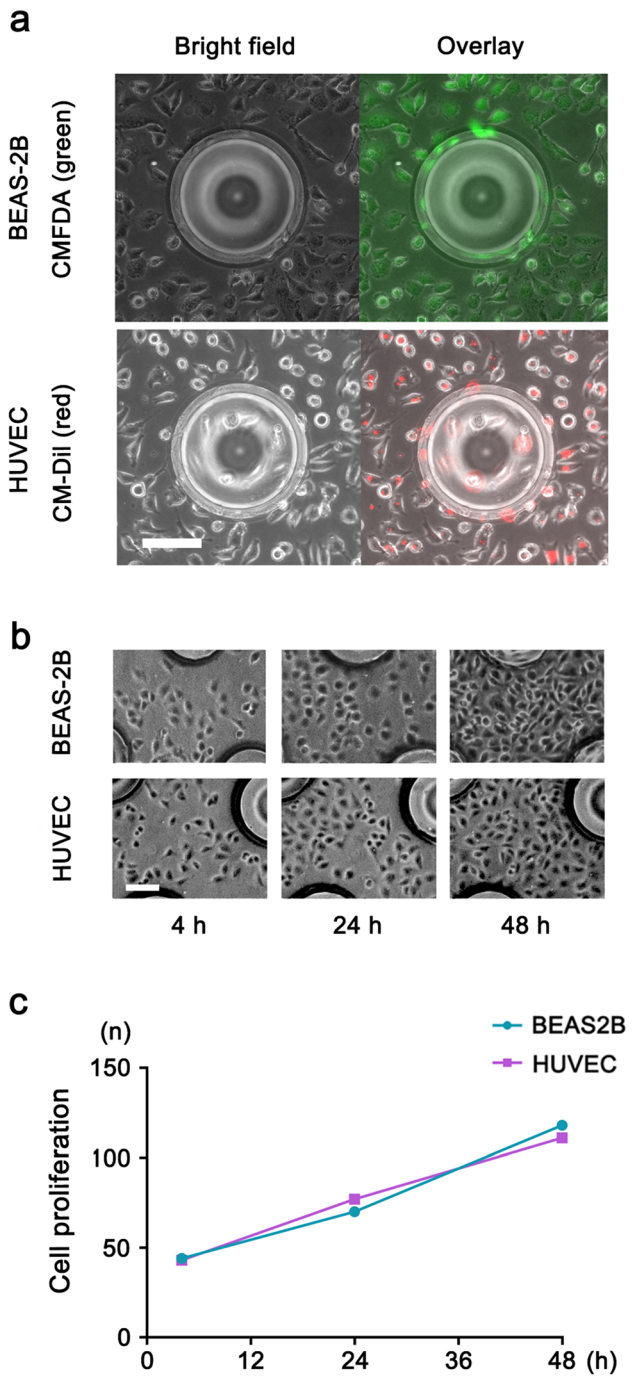

Fig. 3 **a** Live cell staining under an optical microscope. BEAS-2B cells were labelled with CMFDA (green), and HUVECs were labelled with CM-Dil (red). **b** and **c** Growth of cells at different time. Scale bar = 200 μM

[26]. In response to repeated smoke exposure, there was a reduction in several apical junction complexes (AJCs) in pulmonary epithelium [8, 27]. After continuous CSE exposure, there was alternation in the expression of several *AJC* genes. The mRNA expression of IL-6 and TNF-α was significantly up-regulated in BEAS-2B cells subject to CSE exposure. In addition, the mRNA levels of *CLDN1*, *OCLD*, *β-catenin* and *CDH1* were significantly down-regulated. Additionally, the expression of *CLDN-7* and *CLDN-8* genes was up-regulated (Fig. 5).

Endothelial cells from different tissues were believed to vary in permeability. For example, pulmonary endothelium was not a passive barrier to gas exchange [28]; however, it was metabolically active serving as a key mediator of inflammation [29]. Hence, we determined the expression of AJCs and inflammatory cytokines in HUVEC cell lines using the same method. The mRNA levels of *IL-6* and *TNF-α* showed a significant increase, which was consistent with the ELISA results. The inflammatory regulatory function of HUVECs was manifested as the endothelium cells were in direct contact with medium containing CSE in the on-chip model. The mRNA levels of *CLDN1*, *CLDN7*, *CLDN8*, *OCLD*, β-catenin and *CDH5* were significantly down-regulated in the CS stimulation group treated with the highest concentration. CLDN1, CLDN7 and CLDN8 levels did not show a significant dose-dependent relationship in the CS stimulation groups treated with different concentrations compared with that in the NT group. In future, further studies were required to further investigate the potential mechanism (Fig. 6).

CSE promoted epithelial interstitial transformation and oncogene activation

EMT is a crucial process during embryogenesis (EMT type 1), which could also be induced as a consequence of continuous stimulus and inflammation [30]. Tissue fibrosis (EMT type 2) and hyper-vascularity (EMT type 3) are relevant to malignancy, which is identified in one-third of patients with metastatic lung cancer and in approximately 23% of nonsmall cell lung cancer cells [7, 31]. EMT is usually described as the transition of epithelial cells to cells with a mesenchymal phenotype by the identification of prototypical markers (e.g. E-cadherin) [31]. E-cadherin is a critical trans-membrane protein in the AJCs. This protein is inserted in the membrane to mediate cell adhesion. The extracellular domain of E-cadherin connected adjacent cells, while the intracellular domain attached to the actin cytoskeleton. The degeneration of cell adhesion affects its interaction with the actin cytoskeleton, which subsequently leads to the initiation of intracellular signalling cascades. Recent studies demonstrated that E-cadherin and β-catenin were reduced in both cell lines and epithelial cells derived from COPD patients exposed to repetitive CS [32–34]. In the present study, Western blot showed that after continuous CSE exposure (20 μg/mL and 50 μg/mL), the expression levels of E-cadherin and

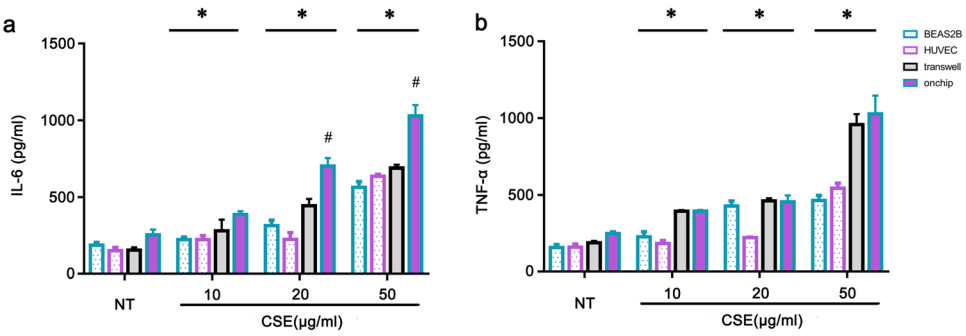

Fig. 4 IL-6 (**a**) and TNF-α (**b**) levels in the supernatant of each group. Data were shown as the means ± standard deviation. *$P < 0.05$ compared to the NT group. # $P < 0.05$ compared to the co-culture group. NT, control group

β-catenin in BEAS-2B cells showed significant decrease (Fig. 7a).

Signal transducer and activator of transcription 3 (STAT3) is an important downstream mediator of IL-6/JAK signalling. It can also provoke EMT in collaboration with K-ras by increasing Snail expression in cancer cells [35, 36]. As mentioned above, IL-6 induced by CSE exposure was detected by ELISA and Real-Time PCR, which indicated that the inflammatory response in the on-chip model was more obvious than that in the conventional co-culture group. Therefore, the phosphorylation level of STAT3 in BEAS-2B cells and HUVECs was detected by Western blot. STAT3 was activated by tyrosine phosphorylation. The results showed that p-STAT3 in the two kinds of cells increased gradually after CS stimulation on-chip (Fig. 7b). Both bronchial epithelium and vascular endothelium involved in the inflammatory response.

STAT3 is considered a proto-oncogene and has direct regulatory effects on c-myc and cyclin D1 in tumours [37]. To further investigate the effects of continuous CS exposure on cell proliferation, we determined the expression of p-ERK, c-myc and cyclin D1 levels in BEAS-2B cells. Based on the results, the levels of p-ERK, c-myc and cyclin D1 in BEAS-2B cells were significantly increased after continuous exposure to CS (Fig. 7c). C-myc is a vital member of the myc proto-oncogene family, which plays regulatory roles in tumourigenesis, proliferation and invasion and is overexpressed in a variety of malignant tumours [38]. Cyclin D1 was a key protein that regulates the G1 phase of the cell cycle. The increased expression of cyclin D1 may lead to checkpoint defects in the G1/S phase, which finally resulted in pathogenesis of malignant cancer [39]. Extracellular regulated protein kinase (ERK) signals from key molecular membrane receptors were transmitted to the nucleus. The phosphorylation activated the ERK signalling pathway, followed by cytoplasmic transfer to the nucleus. Also, it could mediate the transcription activation, participate in the maintenance of cell morphology and cytoskeletal construction, and regulate cell proliferation and differentiation, apoptosis, cancer and other biological reactions. These results demonstrated that prolonged CSE exposure may induce abnormal cell proliferation behaviour.

HJC0152 inhibited STAT3 phosphorylation and BEAS-2B cell proliferation

To evaluate the association between STAT3 phosphorylation and cell proliferation, we introduced a STAT3 inhibitor, HJC0152, into the system. HJC0152 is a STAT3 inhibitor that is widely used as an anti-parasitic medicine. In this study, HJC0152 (1 μM) showed no significant cytotoxicity on BEAS-2B and HUVECs (Fig. 8b). In this study, different concentrations (0.5 μM and 1 μM) of HJC0152 in DMEM solution were pumped into the liquid channel after 50 μg/mL CSE exposure.HJC0152 suppressed the phosphorylation of STAT3 induced by CSE in BEAS-2B cells and HUVECs (Fig. 8d) in a dose-dependent manner. The same tendency was observed in the flow cytometry results. HJC0152, an O-alkylamino-tethered derivative of niclosamide, was defined as an inhibitor for STAT3 signalling pathway, which showed satisfactory water solubility and oral bioavailability in vivo. It exerted a significant anticancer effect on tumour growth and invasion in head and neck squamous cell carcinoma [40, 41]. The STAT3 phosphorylation level was significantly down-regulated after treatment with HJC0152. These data indicated that in CSE-transformed BEAS-2B cells, cell proliferation was more vigorous, which was probably associated with the modulation of the expression of cell cycle regulators. The increased fraction in S and G2 phase caused by prolonged CSE exposure was suppressed by HJC0152, which indicated that HJC0152 may interrupt unexpected cell proliferation triggered by CSE.

The proportion of HJC0152 treated cells arrested in S phase was lower than that of the cells subject to CSE

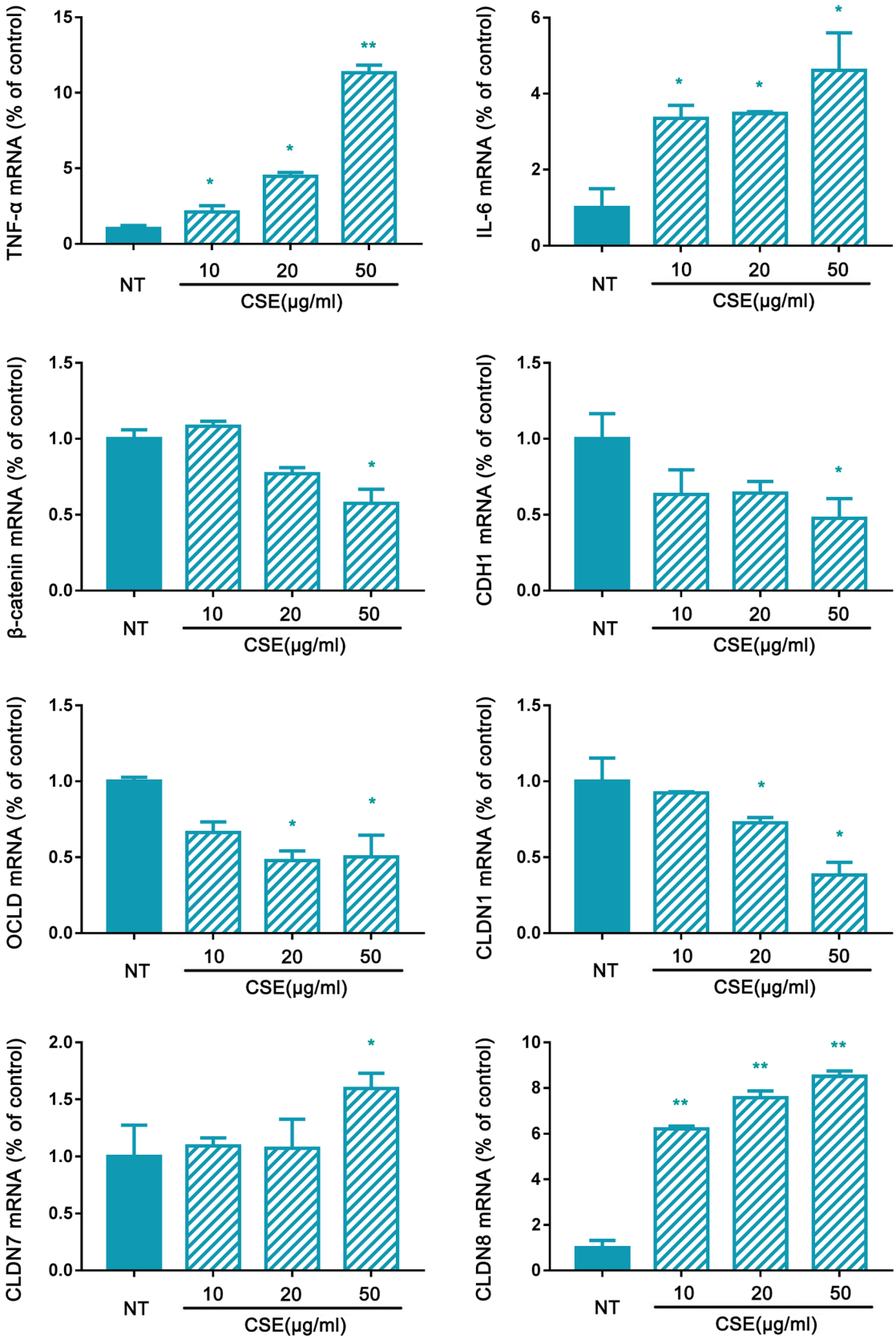

Fig. 5 CSE induced the activation of the inflammatory reaction and altered apical junction complex mRNA expression. Data are shown as the means ± SD. *$P < 0.05$ compared to the NT group; **$P < 0.01$ compared to the NT group

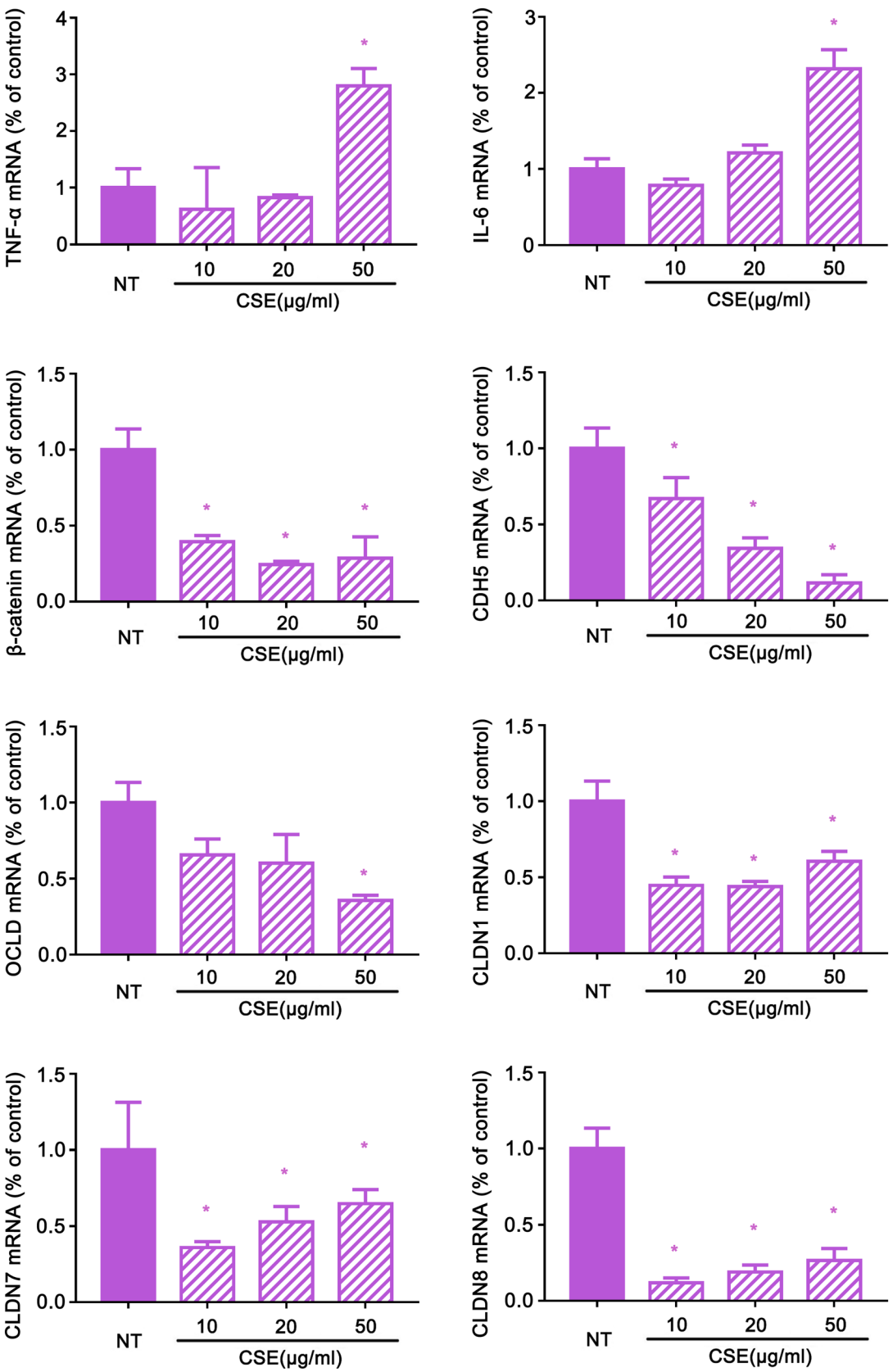

Fig. 6 CSE induced the activation of the inflammatory reaction and altered apical junctional complex mRNA expression in HUVECs. Data were shown as the means ± SD. *$P < 0.05$ compared to the NT group; **$P < 0.01$ compared to the NT group

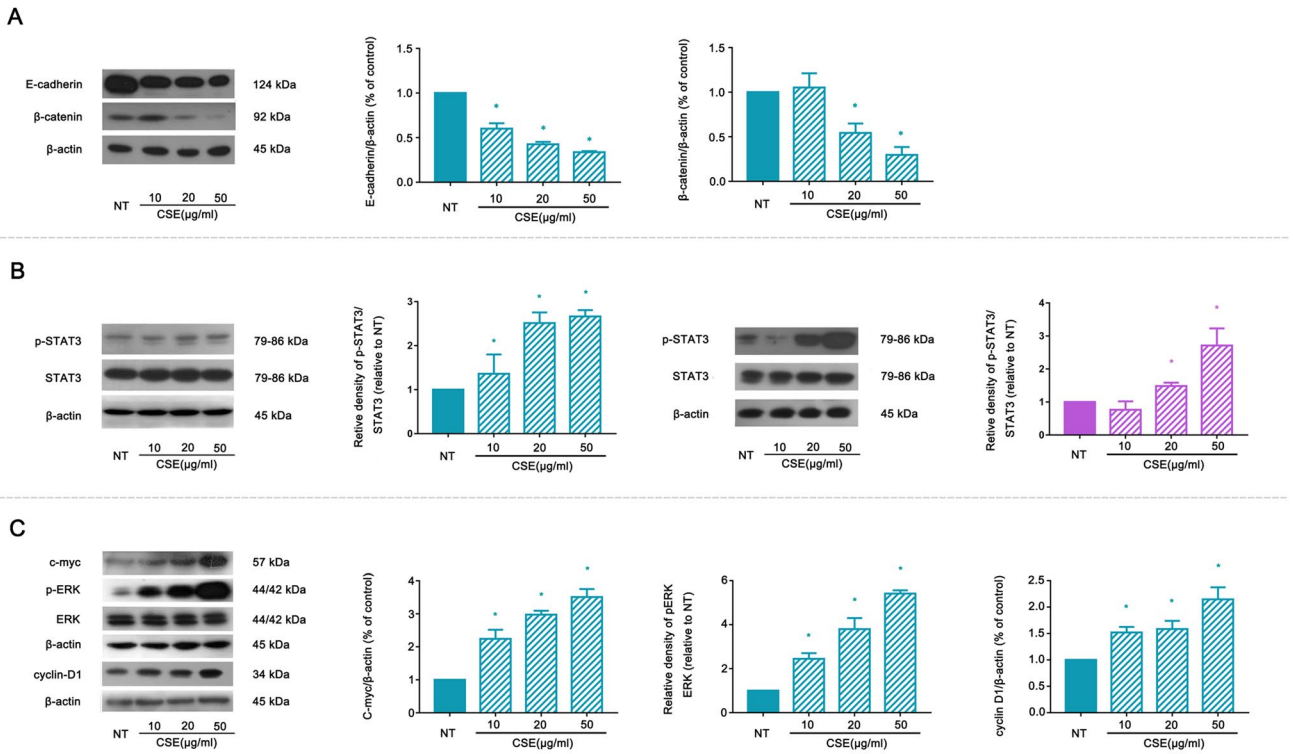

Fig. 7 **a** Western blot analysis of E-cadherin and β-catenin in BEAS-2B cells. CSE decreased the level of E-cadherin and β-catenin. **b** Western blot analysis for the phosphorylation of STAT3 in BEAS-2B cells and HUVECs. CSE induced the phosphorylation of STAT3 without affecting STAT3 expression. **c** Activation of oncogenes c-myc, p-ERK and cyclin D1 in BEAS-2B cells after CSE exposure. $^{*}P < 0.05$ compared to the NT group

exposure, but the proportion of cells arrested in G1 phase was higher than that subject to CSE exposure. The cell cycle checkpoint function was restored to a certain extent (Fig. 8e). However, HJC1052 showed no significant effects on the expression of p-ERK, indicating that HJC1052 had no significant inhibitory effects on the ERK pathway in the CSE-exposed BEAS-2B cells. In addition, the regulation of cyclin was mainly achieved by inhibiting the phosphorylation of STAT3. Western blot revealed that sequential administration of HJC0152 after smoke exposure could up-regulate the expression of E-cadherin rather than β-catenin (Fig. 8f). Taken together, we concluded that HJC0152 may reverse the EMT process induced by CSE exposure.

There are some limitations in our study. First, the cells used in this study were not primary cells obtained from COPD patients, and we could not explore a natural process of malignant tumourigenesis. Future studies with samples derived from CSE-induced COPD patients and COPD-associated lung cancer patients were required to determine whether these changes still exist across different phenotypes of COPD and different subtypes of lung cancer. Second, despite the fact that we have observed the degradation of several AJCs, no definite numerical change was measured, such as trans-epithelial electric resistance. In future, we will try to integrate this detection method into the chip.

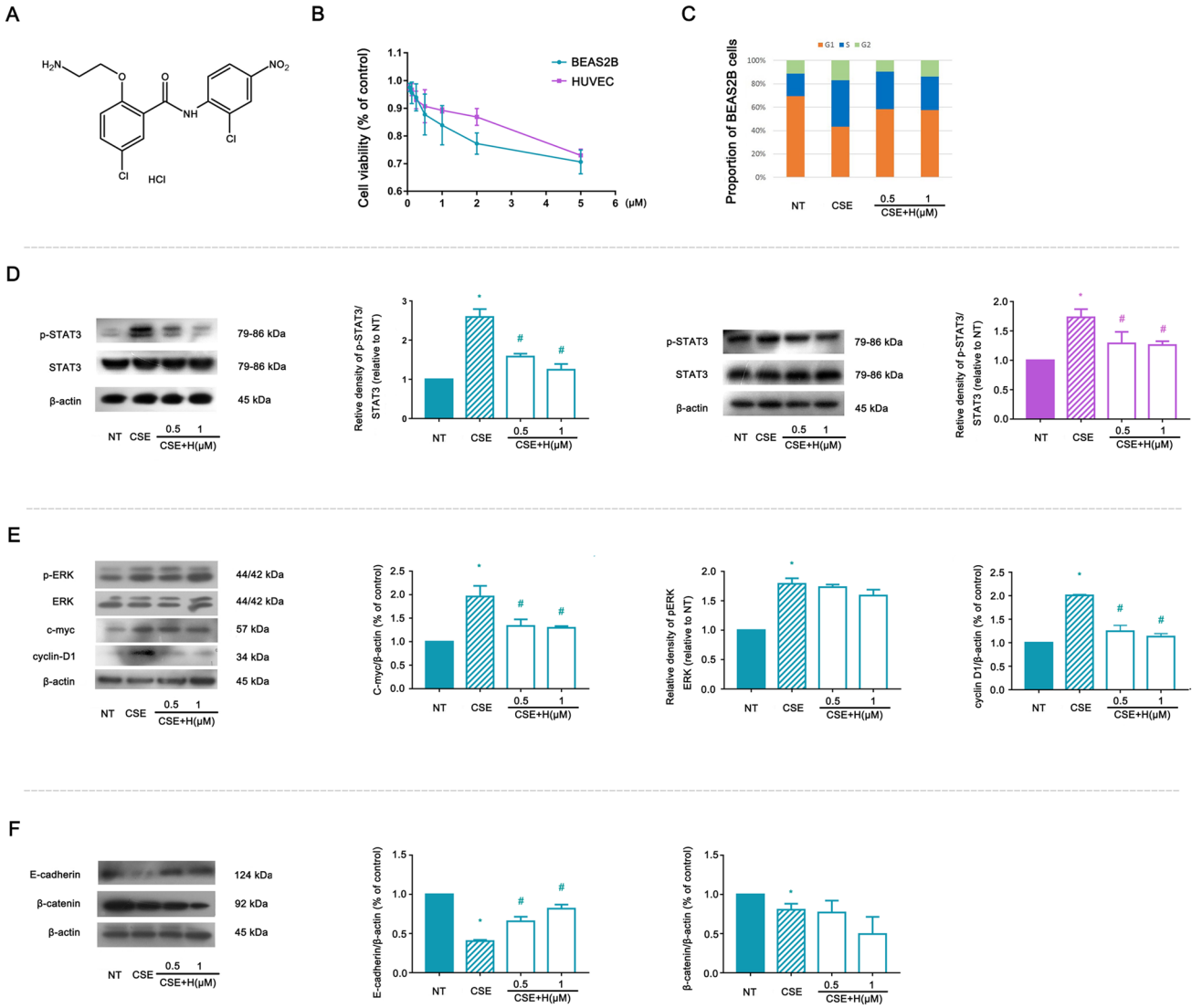

Fig. 8 **a** The molecular formula of HJC0152. **b** Effects of HJC0152 on BEAS-2B cell and HUVEC viability. **c** The overall distribution of cells in each phase of the cell cycle among all the groups. CSE exposure increased the fraction of cells in S and G2 phase and a decreased percentage in G1 phase. **d** HJC0152 suppressed the over phosphorylation of STAT3 induced by CSE in BEAS-2B cells and HUVECs in a dose-dependent manner. **e** HJC0152 decreased the activation of oncogenes c-myc, p-ERK and cyclin D1 in BEAS-2B cells after CSE exposure. **f** HJC0152 increased the level of E-cadherin after CSE exposure. # $P<0.05$ compared to the NT group and *$P<0.05$ compared to the CSE group

Conclusion

In this study, we investigated the possible mechanism that linked cigarette smoking-associated COPD and lung cancer upon fabricating a lung-on-a-chip model containing vascular endothelium and bronchial epithelium to mimic the microenvironment of the air–blood interface. Our data showed that CSE exposure induced inflammation in the co-culture system that impacted the AJC and initiated the EMT process in epithelial cells. Prolonged CSE exposure also promoted cell division. These processes were closely related to STAT3 phosphorylation, which potentially contributed to cigarette smoking-associated COPD pathology and tumour-like transformation. The STAT3 inhibitor HJC0152 could slow down the process, which may be a possible candidate to delay the progression of cigarette smoking-associated COPD and its tumour-like transformation.

Author's contribution W.H, S.H, J.Z. and H.M. conceived the concept and experiments. K-T. Y designed some parts of experiment. W.H. and S.Y. carried out the experiment and collected data. W.H. and S.H. wrote the manuscript, and all authors reviewed and commented on the manuscript.

Funding This work was supported by National Natural Science Foundation of China (Grant Nos.81672297; Grant Nos.61701493), Policy Guidance project (International Science and Technology Cooperation) of Jiangsu Province of China (BZ2018040), the Natural Science Foundation of Tianjin, P.R. China (18JCYBJC42100), Hundred Talents Program of the Chinese Academy of Sciences, Project Funded by China Postdoctoral Science Foundation (2019M651959), Postdoctoral Research Funding Program of Jiangsu Province (2018K004B).

Data availability All data generated or analysed during this study are included in this published article.

Compliance with ethical standards

Conflict of interest The authors declare that they have no conflict of interest.

Ethics approval and consent to participate No laboratory animals or tissue samples from patients were used in this study. This study was performed in line with the principles of the Declaration of Helsinki. Approval was granted by the Ethics Committee of The Second Hospital of Jilin University.

Consent for publication Not applicable.

References

1. Hogg JC, Timens W (2009) The pathology of chronic obstructive pulmonary disease. Annu Rev Pathol 4:435–459. https://doi.org/10.1146/annurev.pathol.4.110807.092145
2. Milara J, Peiró T, Serrano A, Cortijo J (2013) Epithelial to mesenchymal transition is increased in patients with COPD and induced by cigarette smoke. Thorax 68(5):410–420. https://doi.org/10.1136/thoraxjnl2012-201761
3. Decramer M, Janssens W, Miravitlles M (2012) Chronic obstructive pulmonary disease. Lancet 379(9823):1341–1351. https://doi.org/10.1016/s0140-6736(11)60968-9
4. Alwis KU, de Castro BR, Morrow JC, Blount BC (2015) Acrolein exposure in U.S. tobacco smokers and non-tobacco users: NHANES 2005–2006. Environ Health Perspect 123(12):1302–1308. https://doi.org/10.1289/ehp.1409251
5. Portillo-Lara R, Annabi N (2016) Microengineered cancer-on-a-chip platforms to study the metastatic microenvironment. Lab Chip 16(21):4063–4081. https://doi.org/10.1039/c6lc00718j
6. Atkins MB, Larkin J (2016) Immunotherapy combined or sequenced with targeted therapy in the treatment of solid tumors: current perspectives. J Natl Cancer Inst 108(6):djv414. https://doi.org/10.1093/jnci/djv414
7. Brabletz T, Kalluri R, Nieto MA, Weinberg RA (2018) EMT in cancer. Nat Rev Cancer 18(2):128–134. https://doi.org/10.1038/nrc.2017.118
8. Shaykhiev R, Otaki F, Bonsu P, Dang DT, Teater M, Strulovici-Barel Y, Salit J, Harvey BG, Crystal RG (2011) Cigarette smoking reprograms apical junctional complex molecular architecture in the human airway epithelium in vivo. Cell Mol Life Sci 68(5):877–892. https://doi.org/10.1007/s00018-010-0500-x
9. Wang DC, Shi L, Zhu Z, Gao D, Zhang Y (2017) Genomic mechanisms of transformation from chronic obstructive pulmonary disease to lung cancer. Semin Cancer Biol 42:52–59. https://doi.org/10.1016/j.semcancer.2016.11.001
10. Houghton AM (2013) Mechanistic links between COPD and lung cancer. Nat Rev Cancer 13(4):233–245. https://doi.org/10.1038/nrc3477
11. Sundarakrishnan A, Chen Y, Black LD, Aldridge BB, Kaplan DL (2018) Engineered cell and tissue models of pulmonary fibrosis. Adv Drug Deliv Rev 129:78–94. https://doi.org/10.1016/j.addr.2017.12.013
12. Marusyk A, Polyak K (2010) Tumor heterogeneity: causes and consequences. Biochim Biophys Acta 1805(1):105–117. https://doi.org/10.1016/j.bbcan.2009.11.002
13. Benam KH, Villenave R, Lucchesi C, Varone A, Hubeau C, Lee HH, Alves SE, Salmon M, Ferrante TC, Weaver JC, Bahinski A, Hamilton GA, Ingber DE (2016) Small airway-on-a-chip enables analysis of human lung inflammation and drug responses in vitro. Nat Methods 13(2):151–157. https://doi.org/10.1038/nmeth.3697
14. Huh D, Kim HJ, Fraser JP, Shea DE, Khan M, Bahinski A, Hamilton GA, Ingber DE (2013) Microfabrication of human organs-on-chips. Nat Protoc 8(11):2135–2157. https://doi.org/10.1038/nprot.2013.137
15. Aghapour M, Raee P, Moghaddam SJ, Hiemstra PS, Heijink IH (2018) Airway epithelial barrier dysfunction in COPD: role of cigarette smoke exposure. Am J Respir Cell Mol Biol 58(2):157–169
16. Yu J, Ma Z, Shetty S, Ma M, Fu J (2016) Selective HDAC6 inhibition prevents TNF-alpha-induced lung endothelial cell barrier disruption and endotoxin-induced pulmonary edema. Am J Physiol Lung Cell Mol Physiol 311(1):L39–L47. https://doi.org/10.1152/ajplung.00051.2016
17. Sohal SS (2017) Epithelial and endothelial cell plasticity in chronic obstructive pulmonary disease (COPD). Respir Investig 55(2):104–113. https://doi.org/10.1016/j.resinv.2016.11.006
18. Xu X, Farach-Carson MC, Jia X (2014) Three-dimensional in vitro tumor models for cancer research and drug evaluation. Biotechnol Adv 32(7):1256–1268. https://doi.org/10.1016/j.biotechadv.2014.07.009
19. Benam KH, Novak R, Nawroth J, Hirano-Kobayashi M, Ferrante TC, Choe Y, Prantil-Baun R, Weaver JC, Bahinski A, Parker KK, Ingber DE (2016) Matched-comparative modeling of normal and diseased human airway responses using a micro-engineered breathing lung chip. Cell Syst 3(5):456–466. https://doi.org/10.1016/j.cels.2016.10.003
20. Dolega ME, Abeille F, Picollet-D'hahan N, Gidrol X (2015) Controlled 3D culture in Matrigel microbeads to analyze clonal acinar development. Biomaterials 52:347–357. https://doi.org/10.1016/j.biomaterials.2015.02.042
21. Huh D, Matthews BD, Mammoto A, Montoya-Zavala M, Hsin HY, Ingber DE (2010) Reconstituting organ-level lung functions on a chip. Science 328(5986):1662–1668. https://doi.org/10.1126/science.1188302
22. Song P, Tng DJ, Hu R, Lin G, Meng E, Yong KT (2013) An electrochemically actuated MEMS device for individualized drug delivery: an in vitro study. Adv Healthc Mater 2(8):1170–1178. https://doi.org/10.1002/adhm.201200356
23. Ochs M, Nyengaard JR, Jung A, Knudsen L, Voigt M, Wahlers T, Richter J, Gundersen HJ (2004) The number of alveoli in the human lung. Am J Respir Crit Care Med 169(1):120–124. https://doi.org/10.1164/rccm.200308-1107OC
24. Xu Z, Li E, Guo Z, Yu R, Hao H, Xu Y, Sun Z, Li X, Lyu J, Wang Q (2016) Design and construction of a multi-organ microfluidic chip mimicking the in vivo microenvironment of lung cancer

metastasis. ACS Appl Mater Interfaces 8(39):25840–25847. https://doi.org/10.1021/acsami.6b08746
25. Lv XJ, Du YW, Hao YQ, Su ZZ, Zhang L, Zhao LJ, Zhang J (2016) RNA-binding motif protein 5 inhibits the proliferation of cigarette smoke-transformed BEAS-2B cells through cell cycle arrest and apoptosis. Oncol Rep 35(4):2315–2327. https://doi.org/10.3892/or.2016.4551
26. Weibel ER (1964) A morphometric study on the thickness of the pulmonary air-blood barrier. J Cell Biol 21(3):367–384. https://doi.org/10.1083/jcb.21.3.367
27. Hogg JC, Chu F, Utokaparch S, Woods R, Elliott WM, Buzatu L, Cherniack RM, Roger RM, Sciurba FC, Coxson HO, Paré PD (2004) The nature of small-airway obstruction in chronic obstructive pulmonary disease. N Engl J Med 350(26):2645–2653
28. Utoguchi N, Mizuguchi H, Dantakean A, Makimoto H, Wakai Y, Tsutsumi Y, Nakagawa S, Mayumi T (1996) Effect of tumour cell-conditioned medium on endothelial macromolecular permeability and its correlation with collagen. Br J Cancer 73:24–28
29. Lu Q, Gottlieb E, Rounds S (2018) Effects of cigarette smoke on pulmonary endothelial cells. Am J Physiol Lung Cell Mol Physiol 314(5):L743–L756
30. Nieto MA, Huang RY, Jackson RA, Thiery JP (2016) Emt: 2016. Cell 166(1):21–45. https://doi.org/10.1016/j.cell.2016.06.028
31. Gurzu S, Turdean S, Kovecsi A, Contac AO, Jung I (2015) Epithelial-mesenchymal, mesenchymal-epithelial, and endothelial-mesenchymal transitions in malignant tumors: an update. World J Clin Cases 3(5):393–404. https://doi.org/10.12998/wjcc.v3.i5.393
32. Veljkovic E, Jiricny J, Menigatti M, Rehrauer H, Han W (2011) Chronic exposure to cigarette smoke condensate in vitro induces epithelial to mesenchymal transition-like changes in human bronchial epithelial cells, BEAS-2B. Toxicol In Vitro 25(2):446–453. https://doi.org/10.1016/j.tiv.2010.11.011
33. Nishida K, Brune KA, Putcha N, Mandke P, O'Neal WK, Shade D, Srivastava V, Wang M, Lam H, An SS, Drummond MB, Hansel NN, Robinson DN, Sidhaye VK (2017) Cigarette smoke disrupts monolayer integrity by altering epithelial cell-cell adhesion and cortical tension. Am J Physiol Lung Cell Mol Physiol 313(3):L581–L591. https://doi.org/10.1152/ajplung.00074.2017
34. Ward C, Forrest IA, Murphy DM, Johnson GE, Robertson H, Cawston TE, Fisher AJ, Dark JH, Lordan JL, Kirby JA, Corris PA (2005) Phenotype of airway epithelial cells suggests epithelial to mesenchymal cell transition in clinically stable lung transplant recipients. Thorax 60(10):865–871. https://doi.org/10.1136/thx.2005.043026
35. Saitoh M, Endo K, Furuya S, Minami M, Fukasawa A, Imamura T, Miyazawa K (2016) STAT3 integrates cooperative Ras and TGF-beta signals that induce Snail expression. Oncogene 35(8):1049–1057. https://doi.org/10.1038/onc.2015.161
36. D'Amico S, Shi J, Martin BL, Crawford HC, Petrenko O, Reich NC (2018) STAT3 is a master regulator of epithelial identity and KRAS-driven tumorigenesis. Genes Dev 32(17–18):1175–1187. https://doi.org/10.1101/gad.311852.118
37. Aggarwal BB, Kunnumakkara AB, Harikumar KB, Gupta SR, Tharakan ST, Koca C, Dey S, Sung B (2009) Signal transducer and activator of transcription-3, inflammation, and cancer: how intimate is the relationship? Ann N Y Acad Sci 1171:59–76. https://doi.org/10.1111/j.1749-6632.2009.04911.x
38. Lin CY, Loven J, Rahl PB, Paranal RM, Burge CB, Bradner JE, Lee TI, Young RA (2012) Transcriptional amplification in tumor cells with elevated c-Myc. Cell 151(1):56–67. https://doi.org/10.1016/j.cell.2012.08.026
39. Jirawatnotai S, Hu Y, Michowski W, Elias JE, Becks L, Bienvenu F, Zagozdzon A, Goswami T, Wang YE, Clark AB, Kunkel TA, van Harn T, Xia B, Correll M, Quackenbush J, Livingston DM, Gygi SP, Sicinski P (2011) A function for cyclin D1 in DNA repair uncovered by protein interactome analyses in human cancers. Nature 474(7350):230–234. https://doi.org/10.1038/nature10155
40. Wang Y, Wang S, Wu Y, Ren Y, Li Z, Yao X, Zhang C, Ye N, Jing C, Dong J, Zhang K, Sun S, Zhao M, Guo W, Qu X, Qiao Y, Chen H, Kong L, Jin R, Wang X, Zhang L, Zhou J, Shen Q, Zhou X (2017) Suppression of the growth and invasion of human head and neck squamous cell carcinomas via regulating STAT3 signaling and the miR-21/β-catenin axis with HJC0152. Mol Cancer Therap 16(4):578–590. https://doi.org/10.1158/1535-7163.mct-16-0606
41. Chen H, Yang Z, Ding C, Chu L, Zhang Y, Terry K, Liu H, Shen Q, Zhou J (2013) Discovery of O-alkylamino tethered niclosamide derivatives as potent and orally bioavailable anticancer agents. ACS Med Chem Lett 4(2):180–185. https://doi.org/10.1021/ml3003082